Testing Tidal-Torque Theory: II. Alignment of Inertia and Shear and the Characteristics of Proto-haloes

Cristiano Porciani^{1,2}, Avishai Dekel¹ and Yehuda Hoffman¹

- ¹Racah Institute of Physics, The Hebrew University, Jerusalem 91904, Israel
- ² Institute of Astronomy, University of Cambridge, Madingley Road, Cambridge CB3-OHA, UK

28 October 2018

ABSTRACT

We investigate the cross-talk between the two key components of tidal-torque theory, the inertia (I) and shear (T) tensors, using a cosmological N-body simulation with thousands of well-resolved haloes. We find that the principal axes of I and T are strongly aligned, even though I characterizes the proto-halo locally while T is determined by the large-scale structure. Thus, the resultant galactic spin, which plays a key role in galaxy formation, is only a residual due to ~ 10 per cent deviations from perfect alignment of T and I. The T-I correlation induces a weak tendency for the proto-halo spin to be perpendicular to the major axes of T and I, but this correlation is erased by non-linear effects at late times, making the observed spins poor indicators of the initial shear field.

However, the *T-I* correlation implies that the shear tensor can be used for identifying the *positions* and *boundaries* of *proto-haloes* in cosmological initial conditions — a missing piece in galaxy formation theory. The typical configuration is of a prolate proto-halo lying perpendicular to a large-scale high-density ridge, with the surrounding voids inducing compression along the major and intermediate inertia axes of the proto-halo. This leads to a transient sub-halo filament along the large-scale ridge, whose sub-clumps then flow along the filament and merge into the final halo.

The centres of proto-haloes tend to lie in $\sim 1\sigma$ over-density regions, but their association with linear density maxima smoothed on galactic scales is vague: only ~ 40 per cent of the proto-haloes contain peaks within them. Several other characteristics distinguish proto-haloes from density peaks, e.g., they tend to compress along two principal axes while many peaks compress along three axes.

Key words: cosmology: dark-matter - cosmology: large-scale structure of Universe - cosmology: theory - galaxies: formation - galaxies: haloes - galaxies: structure

1 INTRODUCTION

The angular-momentum properties of a galaxy system must have had a crucial role in determining its evolution and final type. A long history of research, involving Hoyle (1953) and Peebles (1969), led to a 'standard' theory for the origin of angular momentum in the cosmological framework of hierarchical structure formation, the tidal-torque theory (hereafter TTT), as put together by Doroshkevich (1970) and White (1984). Special interest in the subject has been revived recently because of an 'angular-momentum crisis', arising from cosmological simulations of galaxy formation which seem to yield luminous galaxies that are significantly smaller, and of much less angular momentum than observed disc galaxies (Navarro, Frenk & White 1995; Navarro & Steinmetz 1997, 2000). Another current motivation comes from weak

lensing studies, where the intrinsic distribution and alignment of galaxy shapes, which may be derived from TTT, play an important role in interpreting the signal (Croft & Metzler 2000; Heavens, Refregier & Heymans 2000; Catelan, Kamionkowski & Blandford 2001; Catelan & Porciani 2001; Crittenden et al. 2001).

These add a timely aspect to the motivation for revisiting the classical problem of angular momentum, in an attempt to sharpen and deepen our understanding of its various components and how they work together. In particular, this effort should start from the acquisition of angular momentum by dark-matter haloes, despite the misleading apparent impression that this part of the theory is fairly well understood. The basic notion of TTT is that most of the angular momentum is being gained gradually by proto-haloes in the linear regime of density fluctuations growth, due to

tidal torques from neighboring fluctuations. This process is expected to continue as long as the proto-halo is expanding. Once it decouples from the expanding background and turns around to non-linear collapse and virialization, only little angular momentum is expected to be tidally exchanged between haloes. It is commonly assumed that the baryonic material, which in general follows the dark-matter distribution inside each proto-halo, gains a similar specific angular momentum and carries it along when it contracts to form a luminous galaxy at the halo centre. This should allow us to predict galactic spins using the approximate but powerful analytic tools of quasi-linear theory of gravitational instability. Even if angular momentum is transferred from the gas to the dark matter during disc formation, the initial set-up of angular-momentum distribution in the halo is an important ingredient in the process.

In a series of papers, we evaluate the performance of the TTT approximation, and trace the roles of its various ingredients and the cross-talk between them. We do it using a cosmological N-body simulation with ~ 7300 well-resolved haloes. We find that some of the basic ingredients of standard TTT involve certain unjustified assumptions and that our understanding of the theory is not full. These papers represent attempts to clarify some of these controversial issues. In Paper I (Porciani, Dekel & Hoffman 2001), we evaluate how well does the approximation predict the final spin of a halo, given full knowledge of the corresponding initial protohalo and the cosmological realization. In the present paper (Paper II), we attempt a deeper level of understanding of the origin of halo angular momentum, by investigating the relation between the different components of TTT. We find that this study connects to the fundamental open question of how to identify a proto-halo in a given realization of initial conditions, and how proto-haloes evolve via collapse and mergers to the present virialized haloes. While the current discussion of proto-haloes and their evolution is limited to first results, a more detailed analysis will be reported in future papers. In Paper III (Porciani & Dekel in preparation), the standard scaling relation of TTT is revised, based on our finding that the shear tensor is weakly correlated with the density at the proto-halo centre of mass. This scaling relation is used to predict the typical angular-momentum profile of haloes (Dekel et al. 2001; Bullock et al. 2001b), and to provide a simple way to incorporate angular momentum in semi-analytic models of galaxy formation (Maller, Dekel & Somerville 2002).

According to TTT, the angular momentum of a halo is due to the cross-talk between two key players: the inertia tensor I, describing the quadrupole structure of the protohalo, and the shear tensor T, representing the external tidal field exerting the torque. There is a controversy in the literature regarding the correlation between these two components, which makes a big difference in the outcome. In applications of TTT, it has commonly been assumed that I and T are uncorrelated (e.g. Hoffman 1986a,b; Heavens & Peacock 1988; Steinmetz & Bartelmann 1995; Catelan & Theuns 1996), based on the argument that the former is local and the latter must be dominated by external sources. Lee & Pen (2000, hereafter LP00), based on simulations with limited resolution, have raised some doubts concerning this assumption. Other applications have made the assumption that the present-day halo angular momentum correlates

with the shear tensor of the initial conditions (LP00; Pen et al. 2000; Crittenden et al. 2001). This involves assuming both a strong correlation at the initial conditions and that this correlation survives the non-linear evolution at late times. In this paper, we investigate the validity of these assumptions, and find surprising results that shed new light on the basic understanding of TTT.

One of our pleasant surprises is that a high degree of correlation between T and I leads to progress in a more general problem, that of identifying proto-haloes in the initial conditions. Despite the impressive progress made in analysing the statistics of peaks in Gaussian random density fields (Bardeen et al. 1986; Hoffman 1986b; Bond & Myers 1996), given a realization of such initial conditions we do not have a successful recipe for identifying the proto-halo centers and the Lagrangian region about them which will end up in the final virialized halo. We find that proto-haloes are only vaguely associated with density peaks. Straightforward ideas for identifying the boundaries, such as involving iso-density or iso-potential contours (Bardeen et al. 1986; Hoffman 1986b, 1988b; Heavens & Peacock 1988; Catelan & Theuns 1996), do not provide a successful algorithm (van de Weygaert & Babul 1994; Bond & Myers 1996). These are key missing ingredients in a full theory for the origin of angular momentum as well as for more general aspects of galaxy formation theory. We make here the first steps towards an algorithm that may provide the missing pieces.

The outline of this paper is as follows: In $\S 2$ we summarize the basics of linear tidal-torque theory. In $\S 3$ we describe the simulation and halo finder, and the implementation of TTT to proto-haloes. In $\S 4$ we address the correlation between the shear field and the inertia tensor of the proto-halo. In $\S 5$ we show examples of the T-I correlation, and address the implications on the characteristics of proto-halo regions and how they evolve. In $\S 6$ we refer to other properties of proto-haloes. In $\S 7$ we address the correlation between the shear field and the spin direction. In $\S 8$ we discuss our results and conclude.

2 TIDAL-TORQUE THEORY

Here is a brief summary of the relevant basics of tidal-torque theory, which is described in some more detail in Paper I.

The framework is the standard FRW cosmology in the matter-dominated era, with small density fluctuations that grow by gravitational instability. Given a proto-halo, a patch of matter occupying an Eulerian volume γ that is destined to end up in a virialized halo, the goal is to compute its angular momentum about the centre of mass, to the lowest non-vanishing order in perturbation theory. The angular momentum at time t is

$$\mathbf{L}(t) = \int_{\gamma} \rho(\mathbf{r}, t) \left[\mathbf{r}(t) - \mathbf{r}_{cm}(t) \right] \times \left[\mathbf{v}(t) - \mathbf{v}_{cm}(t) \right] d^{3}r, \quad (1)$$

where \mathbf{r} and \mathbf{v} are the position and peculiar velocity, and the subscript cm denotes centre-of-mass quantities. Then, in comoving units $\mathbf{x} = \mathbf{r}/a(t)$,

$$\mathbf{L}(t) = \bar{\rho}(t)a^{5}(t) \int_{\gamma} \left[1 + \delta(\mathbf{x}, t)\right] \left[\mathbf{x}(t) - \mathbf{x}_{cm}(t)\right] \times \dot{\mathbf{x}}(t) d^{3}x,$$
(2)

where $\delta(\mathbf{x},t)$ is the density fluctuation field relative to the average density $\bar{\rho}(t)$, a(t) is the universal expansion factor, and the term proportional to $\mathbf{v}_{\rm cm}$ vanished. A dot denotes a derivative with respect to cosmic time t.

The comoving Eulerian position of each fluid element is given by its initial, Lagrangian position \mathbf{q} plus a displacement: $\mathbf{x} = \mathbf{q} + \mathbf{S}(\mathbf{q},t)$. When fluctuations are sufficiently small, or when the flow is properly smoothed, the mapping $\mathbf{q} \to \mathbf{x}$ is reversible such that the flow is laminar. Then the Jacobian determinant $J = ||\partial \mathbf{x}/\partial \mathbf{q}||$ does not vanish, and the continuity equation implies $1 + \delta[\mathbf{x}(\mathbf{q},t)] = J^{-1}(\mathbf{q},t)$. Substituting in Eq. (2) one obtains

$$\mathbf{L}(t) = a^{2}(t)\,\bar{\rho}_{0}a_{0}^{3}\int_{\Gamma}\left[\mathbf{q} - \bar{\mathbf{q}} + \mathbf{S}(\mathbf{q}, t) - \bar{\mathbf{S}}\right] \times \dot{\mathbf{S}}(\mathbf{q}, t)\,d^{3}q\,,$$
(3)

where barred quantities are averages over \mathbf{q} in Γ , the Lagrangian region corresponding to γ . The displacement \mathbf{S} is now spelled out using the Zel'dovich approximation (Zel'dovich 1970), $\mathbf{S}(\mathbf{q},t) = -D(t) \nabla \Phi(\mathbf{q})$, where $\Phi(\mathbf{q}) = \phi(\mathbf{q},t)/4\pi G\bar{\rho}(t)a^2(t)D(t)$ (with G Newton's gravitational constant), and $\phi(\mathbf{q},t)$ is the gravitational potential. Substituting in Eq. (3) one obtains

$$\mathbf{L}(t) = -a^2(t)\dot{D}(t)\,\bar{\rho}_0 a_0^3 \int_{\Gamma} (\mathbf{q} - \bar{\mathbf{q}}) \times \nabla\Phi(\mathbf{q}) \,d^3q \,. \tag{4}$$

The explicit growth rate is $L \propto a^2(t)\dot{D}(t)$, which is $\propto t$ as long as the universe is Einstein-de Sitter, or close to flat (and matter dominated).

Next, assume that the potential is varying smoothly within the volume Γ , such that it can be approximated by its *second-order* Taylor expansion about the centre of mass,*

$$\Phi(\mathbf{q}') \simeq \Phi(\mathbf{0}) + \frac{\partial \Phi}{\partial q_i'} \Big|_{\mathbf{q}'=0} q_i' + \frac{1}{2} \frac{\partial^2 \Phi}{\partial q_i' \partial q_j'} \Big|_{\mathbf{q}'=0} q_i' q_j', \quad (5)$$

where $\mathbf{q}' \equiv \mathbf{q} - \bar{\mathbf{q}}$. Substituting in Eq. (4), one obtains the basic TTT expression for the *i*th Cartesian component:

$$L_i(t) = a^2(t)\dot{D}(t)\,\epsilon_{ijk}\,\mathcal{D}_{il}\,I_{lk}\,,\tag{6}$$

where ϵ_{ijk} is the antisymmetric tensor, and the two key quantities are the *deformation* tensor at $\mathbf{q}' = 0$,

$$\mathcal{D}_{ij} = -\left. \frac{\partial^2 \Phi}{\partial q_i' \partial q_j'} \right|_{\mathbf{g}'=0}, \tag{7}$$

and the *inertia* tensor of Γ ,

$$I_{ij} = \bar{\rho}_0 a_0^3 \int_{\Gamma} q_i' \, q_j' \, d^3 q' \,. \tag{8}$$

Note that only the traceless parts of the two tensors matter for the cross product in Eq. (6). These are the velocity shear or tidal tensor, $T_{ij} = \mathcal{D}_{ij} - (\mathcal{D}_{ii}/3)\delta_{ij}$, and the traceless quadrupolar inertia tensor, $I_{ij} - (I_{ii}/3)\delta_{ij}$. Thus, to the first non-vanishing order, angular momentum is transferred to the proto-halo by the gravitational coupling of the quadrupole moment of its mass distribution with the tidal field exerted by neighboring density fluctuations. The torque depends on the misalignment between the two.

3 TTT IN SIMULATIONS

We summarize here the relevant issues concerning the simulation, the halo finding, and the way we implement TTT. A more detailed description is provided in Paper I.

The N-body simulation was performed as part of the GIF project (e.g., Kauffmann et al. 1999) using the adaptive P³M code developed by the Virgo consortium (Pearce et al. 1995; Pearce & Couchman 1997). As an example, we use a simulation of the τ CDM scenario, in which the cosmology is flat, with density parameter $\Omega_{\rm m}=1$ and Hubble constant $h = 0.5 \ (H_0 = 100 \, h \, \text{km s}^{-1} \, \text{Mpc}^{-1})$. The power spectrum of initial density fluctuations is CDM with shape parameter $\Gamma = 0.21$, normalized to $\sigma_8 = 0.51$ today. The simulation was performed in a periodic cubic box of side $84.55 h^{-1}\mathrm{Mpc}$, with 256^3 particles of $1.0 \times 10^{10} h^{-1} M_{\odot}$ each. Long-range gravitational forces were computed on a 512³ mesh, while short-range interactions were calculated as in Efstathiou & Eastwood (1981). At late times $(z \lesssim 3)$, the gravitational potential asymptotically matches a Plummer law with softening $\epsilon = 36 \, h^{-1}$ kpc. The simulation started at z = 50 and ended at z = 0. The initial conditions were generated by displacing particles according to the Zel'dovich approximation from an initial stable 'glass' state (e.g. White 1996). More details are in Jenkins et al. (1998).

Fig. 1 shows a typical halo and its proto-halo, to help illustrating the objects of our analysis. We identify dark-matter haloes at z=0 using a standard friends-of-friends algorithm with a linking length 0.2 in units of the average inter-particle distance. This algorithm identifies regions bounded by a surface of approximately constant density, corresponding to haloes with a mean density contrast $\simeq 180$, in general agreement with spherical perturbations whose outer shells have collapsed recently. We then remove unbound particles from each halo, and consider only haloes which contain more than 100 bound particles. Our results turn out to be insensitive to the removal of unbound particles, which is at a typical level of only a few per cent.

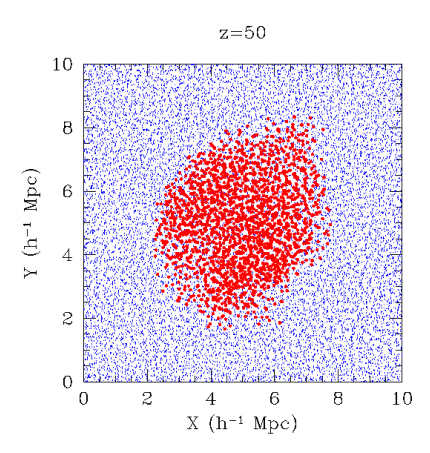
The robustness of our conclusions regarding TTT with respect to the halo-finding algorithm (e.g., friends-of-friends versus fitting a spherical or ellipsoidal density profile, Bullock et al. 2001a) is investigated in another paper in preparation. Note that all the haloes in our current sample are not subclumps of larger host haloes, for which linear theory is not expected to be valid. This excludes about 10 per cent of the haloes that are more massive than $10^{12}\,h^{-1}{\rm M}_{\odot}$ (Sigad et al. 2001).

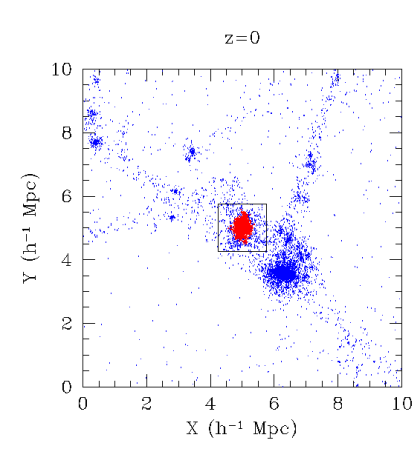
The proto-halo regions Γ are defined by simply tracing all the virialized halo particles, as identified today, into their Lagrangian positions. In most cases, most of the proto-halo mass is contained within a simply connected Lagrangian region, but in some cases (~ 15 per cent) the proto-halo may be divided into two or three compact regions which are connected by thin filaments. Nearly 10 per cent of the proto-haloes are characterized by extended filaments departing from a compact core. A typical case is illustrated in Fig. 1, where we show a halo at z=0 and its proto-halo at z=50, embedded in the surrounding particles in a comoving slice that includes most of the halo particles.

For each proto-halo, we compute the Lagrangian inertia tensor by direct summation over its N particles of mass m

^{*} This is equivalent to assuming that the velocity field is well described by its linear Taylor expansion, i.e., $v_i - \bar{v}_i \simeq \mathcal{D}_{ij} q'_i$.







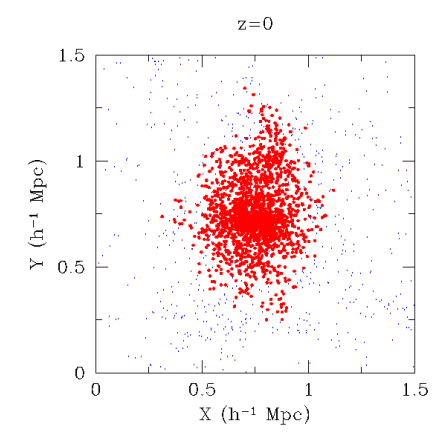


Figure 1. An example of a halo at z=0 (center and right) and its proto-halo at z=50 (left), embedded in the surrounding particles in a comoving slice about the halo centre of mass. The thickness of the slice is 5.4 and $0.9 h^{-1}$ Mpc (comoving) for the left, center and right panels respectively, such that all the halo particles are included. Particles belonging to the halo are marked by filled circles, while points denote background particles. Note that the halo is centred on one clump within a filament, while the neighbouring haloes are not marked. Note also that the proto-halo boundaries do not necessarily follow the orientation of the filament. Initial density contours in the region surrounding the proto-halo are shown in Figure 4.

each:

$$I_{ij} = m \sum_{n=1}^{N} q_i^{'(n)} q_j^{'(n)} , \qquad (9)$$

with $\mathbf{q}^{'(n)}$ the position of the *n*-th particle with respect to the halo centre of mass.

The shear tensor at the proto-halo centre of mass is computed by first smoothing the potential used to generate the initial Zel'dovich displacements, and then differentiating it twice with respect to the spatial coordinates (Method 1). Smoothing is done using a top-hat window function, while derivatives are computed on a grid. The top-hat smoothing radius, in comoving units, is taken to be defined by the halo mass via $(4\pi/3)\bar{\rho}_0 R^3 = M$. In Paper I we also tested two alternative methods for computing the shear tensor: Method 2, in which the smoothing has been replaced by minimal variance fitting, and Method 3, also with minimal variance fitting, but in which we considered only the shear generated by the density perturbations lying outside the proto-halo volume. The TTT predictions for the halo spin based on the three methods were found to be of similar quality at z=0, while Methods 2 and 3 are slightly more accurate at very high redshift. We adopt method 1 here because it does not depend explicitly on the detailed shape of the proto-haloes, which prevents spurious correlations between T and I due to the way T is computed. Also, this is the only method applicable in analytic and semi-analytic modelling.

4 ALIGNMENT OF INERTIA AND SHEAR

In Paper I, we evaluated the success of TTT in predicting the final halo angular momentum for a given proto-halo

embedded in a given tidal environment at the initial conditions. For a deeper understanding of how TTT works, we now proceed to investigate the key players: the inertia and shear tensors and in particular the cross-talk between them. Note, in Eq. (6), that angular momentum is generated only due to *misalignments* of the principal axes of these tensors. It has been assumed, in many occasions, that these two tensors are largely uncorrelated, the inertia tensor being a local property while the shear tensor is dominated by large-scale structure external to the proto-halo (e.g. Hoffman 1986a, 1988a; Heavens & Peacock 1988; Steinmetz & Bartelmann 1995; Catelan & Theuns 1996). Such a lack of correlation would have led to relatively large spins and would have provided a specific statistical framework for TTT. On the other hand, a strong correlation between I and T would have led to relatively small spins, and would have invalidated some of the predictions based on the assumption of independence of I and T. Moreover, a correlation of this sort could provide the missing clue for the special characteristics of the Lagrangian proto-halo regions Γ , those that will eventually evolve into virialized haloes.

We address the correlation between the principal axes of I and T at the proto-halo centres of mass by first showing in Fig. 2 the probability distributions of the cosines of the angles between them. The eigenvectors $\hat{\mathbf{i}}_j$ and $\hat{\mathbf{t}}_k$ are labeled in such a way that the corresponding eigenvalues are ranked $i_1 \geq i_2 \geq i_3$ and $t_1 \leq t_2 \leq t_3$, namely the major axes are denoted by 1 and the minor axes by 3 (and note, for example, that t_1 is the direction of maximum compression). The highest spike (near a cosine of unity) indicates a very

[†] The principal axes of T_{ij} coincide with those of \mathcal{D}_{ij} , because the difference of the two tensors is a scalar matrix.

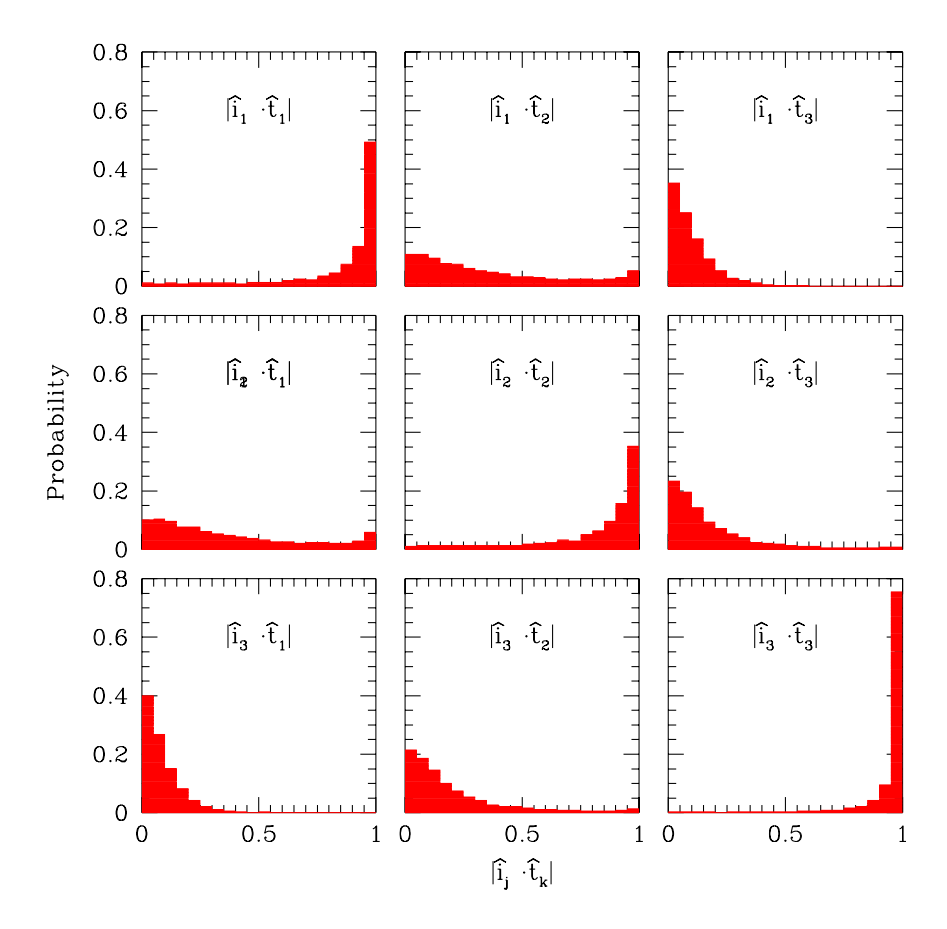


Figure 2. Alignments of I and T. Distributions of the cosine of the angle between the directions of the principal axes of the inertia tensor $(\hat{\mathbf{i}}_j)$ and of the velocity shear tensor $(\hat{\mathbf{t}}_k)$. The corresponding eigenvalues are ordered $i_1 \geq i_2 \geq i_3$ and $i_1 \leq i_2 \leq i_3$, such that 1 denotes the major axis and 3 denotes the minor axis. The first two moments of the distributions are given in Eq. (10) and Eq. (11).

strong alignment between the minor axes of the two tensors, and the second-highest spike refers to a strong alignment between the major axes. The alignment between the intermediate axes is also apparent but somewhat weaker. The peaks near a cosine of zero indicate a significant tendency for orthogonality between the major axis of one tensor and the minor axis of the other. There is a somewhat weaker orthogonality between the intermediate and minor axes, and the weakest orthogonality is between the major and intermediate axes.

The first two moments of these distributions are

$$\mu_{ij} = \langle |\hat{\mathbf{i}}_i \cdot \hat{\mathbf{t}}_j| \rangle = \begin{pmatrix} 0.838 & 0.363 & 0.106 \\ 0.370 & 0.793 & 0.196 \\ 0.091 & 0.206 & 0.935 \end{pmatrix} , \qquad (10)$$

and

$$\nu_{ij} = \langle (\hat{\mathbf{i}}_i \cdot \hat{\mathbf{t}}_j)^2 \rangle = \begin{pmatrix} 0.759 & 0.219 & 0.023 \\ 0.225 & 0.692 & 0.083 \\ 0.017 & 0.089 & 0.895 \end{pmatrix} . \tag{11}$$

Based on the higher-order moments and the number of haloes in the sample, the statistical uncertainty in these mean quantities is between 0.001 and 0.003, depending on the matrix element considered. In order to estimate the systematic errors due to the finite number of particles in each halo, we re-measured the moments considering only the

haloes containing 1000 particles or more. The results agree with those dominated by smaller haloes of \geq 100 particles at the level of a few per cent. For example, we obtain

$$\mu_{ij} = \begin{pmatrix} 0.792 & 0.418 & 0.142 \\ 0.433 & 0.733 & 0.226 \\ 0.117 & 0.243 & 0.907 \end{pmatrix} , \qquad (12)$$

with a typical statistical uncertainty of 0.010.

The values of the matrix elements μ_{ij} and ν_{ij} can be used to quantify the degree of correlation between the shear and inertia tensors. Note that a perfect correlation corresponds to a diagonal, unit matrix both for μ and ν , while perfect independence corresponds to all the elements being equal at 1/2 (for μ) or 1/3 (for ν). Note that, by definition, $\sum_{j} \nu_{ij} = \sum_{i} \nu_{ij} = 1$. To characterize the above matrices with single numbers, we define a correlation parameter for μ_{ij} by

$$c_{\mu} = \frac{1}{9} \sum_{i,j=1}^{3} \frac{\mu_{ij} - 1/2}{\delta_{ij} - 1/2} = \frac{1}{3} + \frac{2}{9} (\mu_{ii} - \sum_{i \neq j} \mu_{ij});$$
 (13)

it obtains the values zero and unity for minimum and maximum correlation respectively. Similarly, we define a corre-

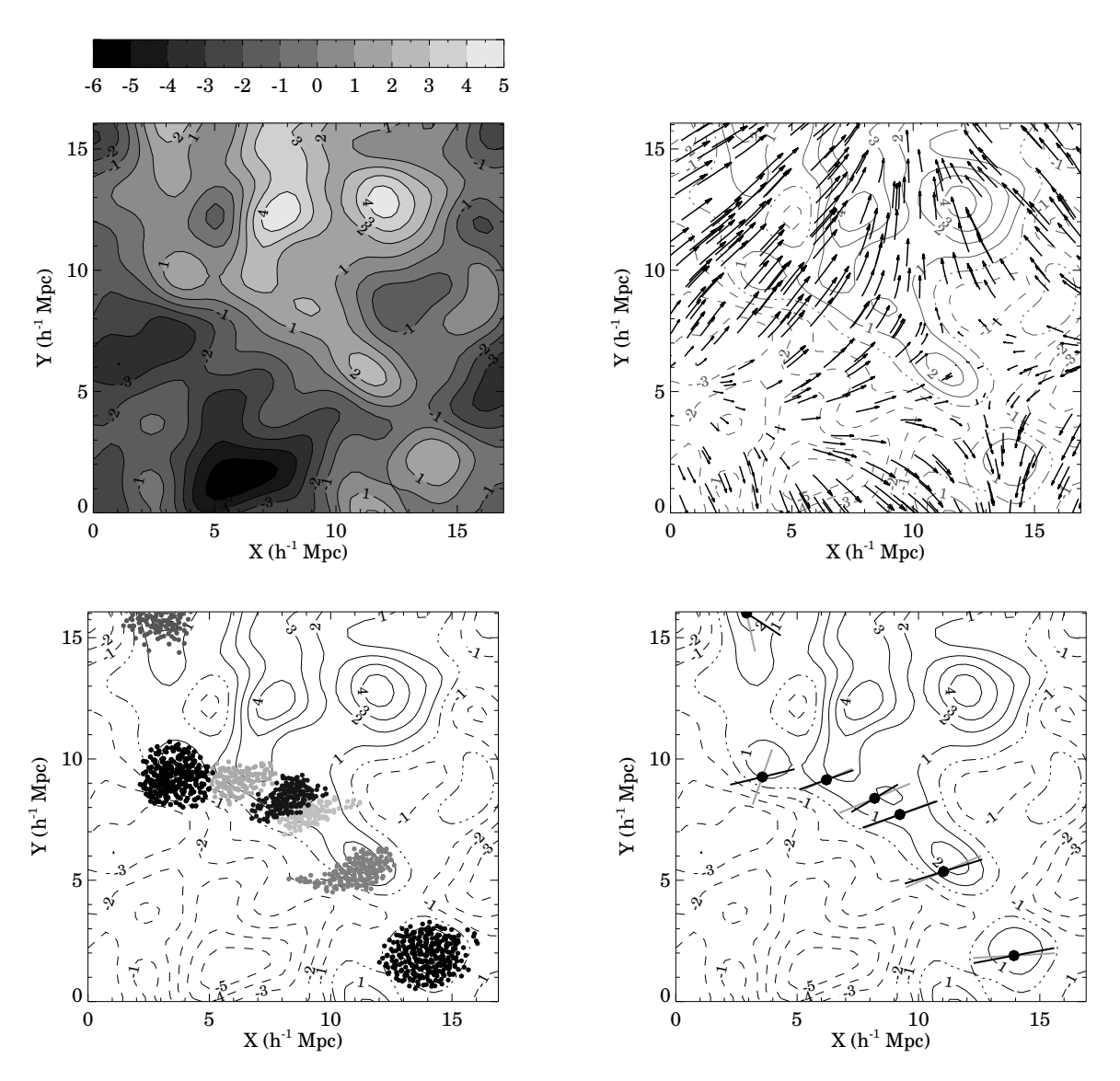


Figure 3. Examples of the correlation between I and T. The top panels show maps of the density (left) and velocity (right) fields, at z = 50, in a section of an X - Y plane from the simulation box. The fields are smoothed with a top-hat window of radius $0.95 h^{-1}$ Mpc corresponding to a 100-particle halo. The contours refer to the density contrast linearly extrapolated to z = 0. The bottom panels show all the proto-haloes whose centres of mass lie within one smoothing length of the plane (A cluster-size halo associated with the high density peaks at the top is not shown because its centre lies further away from the plane). The left panel shows the projection of the proto-halo particle positions. The haloes contain, from left to right, 179, 257, 143, 168, 100, 183, and 300 particles. The right panel shows the projections of the major axes of I (dark lines) and T (light lines) about the centres of mass (filled circles). The line length is proportional to the projection of a unit vector along the major axis on to the X - Y plane. To set the scale, we note, for example, that the principal axis of the inertia tensor of the proto-halo at the centre of the panel lies almost exactly in the plane shown.

lation parameter using ν_{ij} ,

$$c_{\nu} = \frac{1}{9} \sum_{i,j=1}^{3} \frac{\nu_{ij} - 1/3}{\delta_{ij} - 1/3} = \frac{1}{2} (\nu_{ii} - 1) . \tag{14}$$

We find in the simulation $c_{\mu} = 0.61$ and $c_{\nu} = 0.67$, indicating a strong correlation between I and T.

We have repeated the above correlation analysis for the two alternative methods of computing the shear tensor described in §4 of Paper I. When we minimize smoothing and include only the part of the shear tensor that is generated by fluctuations external to the proto-halo (*Method 3*), the correlations are very similar to those obtained with top-hat

smoothing, indicating that these are indeed the correlations of physical significance that we are after. When we minimize smoothing and include the contribution from internal fluctuations ($Method\ 2$), the correlations still show but they get significantly weaker because of the additional noise in the computation of T. Thus, our standard way of computing T ($Method\ 1$) seems to pick up properly the correlation with I, and we proceed with it.

Note that T-I correlations are unavoidable in the framework of the Zel'dovich approximation, where a halo consists by the matter that has shell-crossed. However, the strength of the expected correlations has still to be worked out.

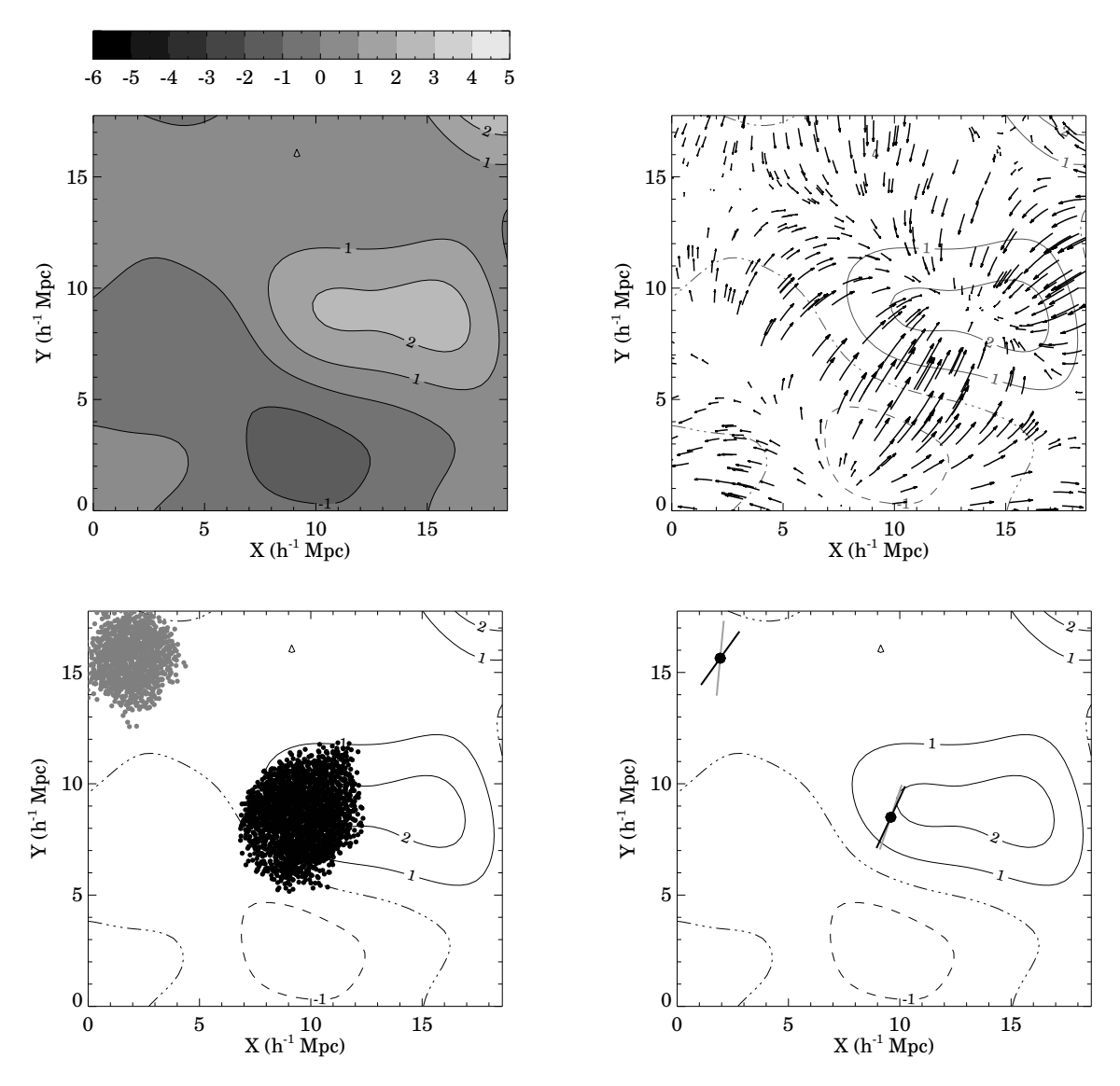


Figure 4. Same as Fig. 3, but for a different region of the simulation, and showing only the haloes of more than 1000 particles. The haloes contain, from left to right, 1065 and 2003 particles. The smoothing length of $2.58 \,h^{-1}{\rm Mpc}$ now corresponds to a 2000-particle proto-halo.

The implication of the T-I alignment is that proto-halo spins are due to small residuals from this correlation. This means that the haloes acquire significantly less angular momentum than one would have expected based on a simple dimensional analysis that ignores the correlation. We quantify the effect by a comparison to an artificial case where the alignments are erased. For each halo in our sample, we randomize the relative directions of the eigenvectors of the inertia and tidal tensors (by a three-dimensional rotation with random Euler angles), and then re-compute the angular momentum using Eq. (6). A vast majority of the haloes, about 88 per cent, are found to be associated with a larger spin after the randomization procedure. The T-I correlation is found to reduce the halo spin amplitude with respect to the randomized case by an average factor of 3.1, with a comparable scatter of 3.2. This heads towards explaining why haloes have such low values of the dimensionless spin parameter, $\lambda \sim 0.035$ on average (Barnes & Efstathiou 1987;

Bullock et al. 2001b), namely a very small rotational energy compared to gravitational or kinetic energy.

5 PROTO-HALO REGIONS

The strong correlation between the principal axes of the inertia and tidal tensors promises very interesting implications on galaxy-formation theory. It indicates that the tidal field plays a key role in determining the locations and shapes of proto-haloes, and therefore may provide a useful tool for identifying proto-haloes in cosmological initial conditions.

As a first step, we try to gain intuitive understanding of the nature of the correlation between T and I by inspecting a few proto-haloes and their cross-talk with their cosmological environment. Fig. 3 and Fig. 4 show a few examples, in regions of the simulation box containing several protohaloes. In the top panels we show maps of the density and velocity fields at the initial conditions, to indicate some of the qualitative properties of the shear field. We focus on a section of one plane at at time, and project the velocity field onto it. The fields are smoothed with a top-hat window corresponding to the typical halo masses shown in that region: in Fig. 3, the smoothing radius is $0.95\,h^{-1}{\rm Mpc}$, to match the haloes that contain 100 to 300 particles each, while in Fig. 4 it is $2.58\,h^{-1}{\rm Mpc}$, to match the haloes of 1000 to 2000 particles. The smoothed density contrast is linearly extrapolated to z=0.

We then introduce, in the bottom panels, the protohaloes and their inertia tensors. We present all the protohaloes whose centres of mass lie within one smoothing length of the plane by showing, in the bottom-left panels, the projection of the proto-halo particle positions onto the plane. We see a tendency for an association between the proto-halo centres of mass and density peaks smoothed on a halo scale, but this association seems to be far from perfect (e.g. near the centre of the frame in Fig. 3). Note that the single plane shown does not allow an accurate identification of the peak location, and therefore a definite evaluation of the association of proto-haloes and peaks cannot be properly addressed by observing these maps. In order to quantify the correlation between proto-haloes and peaks, we identified peaks in the linear density field, smoothed with a top-hat window that contains n (with n=100, 1000 and 10000) particles, and determined the nearest peak to the centre of mass of each of the proto-haloes that contain $n \ (\pm 10 \text{ per cent})$ particles. Independently of the halo mass, we find that only $\sim 35-45$ per cent of the proto-halo centers lie within one smoothing radius from the nearest peak, and $\sim 60-65$ per cent lie within two smoothing radii. We conclude that while the proto-haloes tend to lie in high density regions, their centres do not coincide with the local density maxima, and in fact the spatial correlation between the two is quite weak.

In the bottom-right panels, we stress the projections of the major axes of the inertia and shear tensors about the centres of mass, and indicate by the length of the line the cosine of the angle between the axis and the plane shown. Note, for example, that the major axes of those haloes in Fig. 3 that reside near the centre of the frame and towards the bottom right happen to lie almost perfectly in the plane shown. All the proto-haloes that show a significant deviation from spherical symmetry have their major inertia axis strongly aligned with the first principal shear axis at their centre of mass. This alignment reflects the fact that the largest compression flow towards the centre of the proto-halo is along the major inertia axis of the proto-halo. Indeed, this is exactly what is required in order to compress the elongated proto-halo into the more centrally concentrated and quite spherical configuration identified by the halo finder after collapse and virialization.

The detected alignment is a clear manifestation of the crucial role played by the external shear in determining the shape of the Lagrangian volume of the proto-halo. One way to interpret this alignment is as follows. The compression along the major axis of T is associated with a flow of matter from the vicinity into the proto-halo. This matter comes from relatively large distances and it is therefore responsible for a large inertia moment along this axis in the proto-halo configuration. In contrast, the dilation along the minor axis of T causes matter to be tidally stripped, thus leading to a

relatively small inertia moment of the proto-halo along this axis. This picture, in which the boundaries of the proto-halo are fixed by the push and pull of the external mass distribution, is in some sense the opposite of the common wisdom, where the crucial factor is assumed to be the self-gravity attraction. This other approach, which predicts that collapse first occurs along the minor inertia axis, is based on the simplified model of the collapse of an isolated ellipsoidal perturbation that starts at rest or comoving with the Hubble flow (Lin, Mestel & Shu 1965; Zel'dovich 1965).

Snapshots of the evolution of a typical halo (the same massive halo shown in Fig. 1 and Fig. 4) are shown in Fig. 5. Plotted are the positions at different epochs of the particles that form the halo identified at z=0. The proto-halo first collapses along its major and intermediate inertia axes, giving rise to an elongated structure made of sub-clumps. The final halo is then assembled by merging and accretion along the axis of the elongated filament. This transient sub-halo filament lies along the large-scale filament in which the final halo is embedded (see Fig. 1 and Fig. 4). It indicates that the late stages of halo formation are associated with flows along preferential directions aligned with the cosmic web (see also Colberg et al. 1999).

It has often been assumed that the boundaries of protohaloes could be identified with some threshold iso-density contours about density maxima. (Bardeen et al. 1986; Hoffman 1986b, 1988b; Heavens & Peacock 1988; Catelan & Theuns 1996). In this case, the density distribution in a proto-halo could be approximated by a second-order Taylor expansion of the density profile about the peak. Figures 3 and 4 demonstrate that this assumption is going to fail in most cases shown (except, perhaps, the halo at the bottomright of Fig. 3). In a typical proto-halo, the boundaries are not determined by the self gravity due to the local mass distribution within the proto-halo but rather by the tidal field due to the external mass distribution. Such a proto-halo is typically embedded within a large-scale elongated density ridge, but is not necessarily centred on a local density peak. The compressions exerted by the void regions surrounding the ridge define the compression axes of the shear tensor in directions perpendicular to the ridge, while the tides from the other parts of the ridge cause large-scale dilation along the ridge. The associated push and pull of mass along these directions make the large inertia axes of the proto-halo lie perpendicular to the ridge, and the minor inertia axis lie parallel to the ridge. This understanding should be translated to a practical recipe for identifying the boundaries of proto-haloes. At later stages we also see an internal compression and merging along the filament, namely the minor inertia axis of the proto-halo.

6 OTHER PROPERTIES OF PROTO-HALOES

We continue with a complementary investigation of the properties of proto-haloes, using several different statistics that may, in particular, distinguish them from random Gaussian peaks.

First of all, we study the shapes of the proto-haloes in Lagrangian space using their inertia tensors. A complete description of the statistical properties of the eigenvalues of the inertia tensor (a symmetric, positive definite matrix)

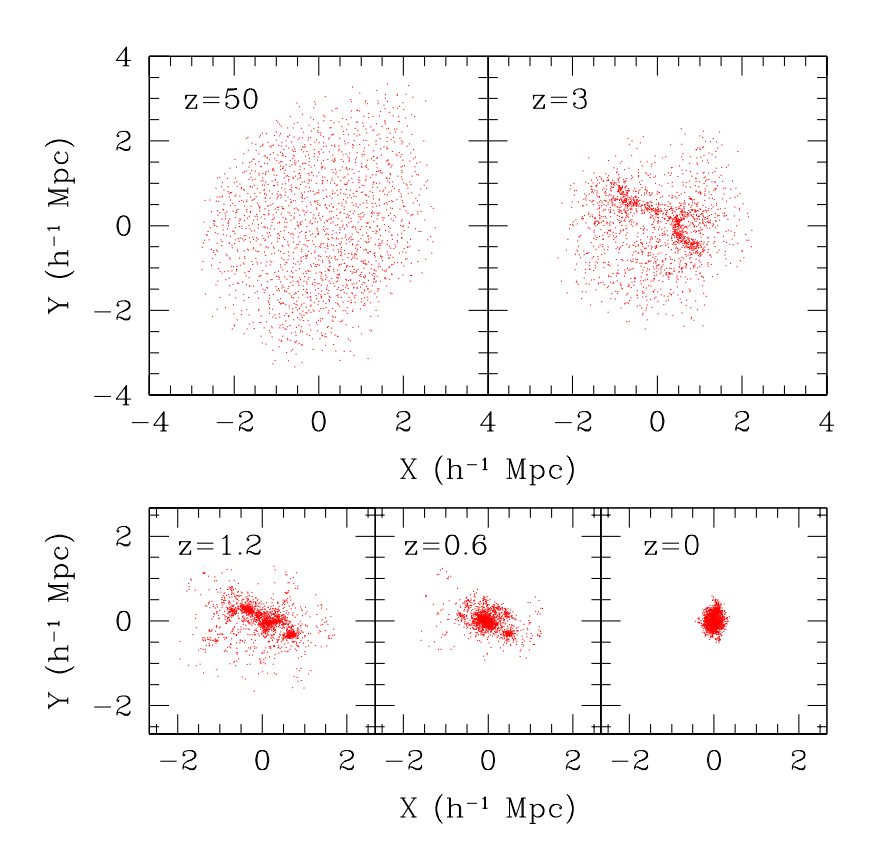


Figure 5. Time evolution of a protohalo. Shown are the projected positions of the halo particles at different redshifts in a fixed comoving box about the centre of mass. The first collapse along the major axis of inertia (and the major axis of the tidal field) leads to the formation of a transient filament, which breaks into sub-clumps. These sub-clumps then flow along the filament and merge into the final halo

can be obtained in terms of the three following parameters: the trace $\tau = i_1 + i_2 + i_3$, the ellipticity $e = (i_1 - i_3)/2\tau$, and the prolateness $p = (i_1 - 2i_2 + i_3)/2\tau$. A perfect sphere has e = p = 0. A flat circular disc (ultimate oblateness) has e = 1/4 and p = -1/4. A thin filament (ultimate prolateness) has e = 1/2 and p = 1/2. Thus, e measures the deviation from sphericity, and p measures the prolateness versus oblateness. In Fig. 6 we show the joint distribution of ellipticity and prolateness, and the probability distribution marginalized along each axis, for our proto-haloes at z = 50. The boundaries $e \geq -p$, $e \geq p$, and $p \geq 3e-1$ arise from the conditions $i_1 \geq i_2$, $i_2 \geq i_3$, and $i_3 \geq 0$, respectively. As a consequence, the data-points populate only a triangle in the e-p plane, with vertices at (0,0), (1/2,1/2) and (1/4,-1/4). This introduces a correlation between e and p at high ellipticities (e > 1/4). We find that only 3 per cent of the protohaloes are nearly spherical, with e < 0.1 (or |p| < 0.1). Most of the proto-haloes, 74 per cent, have moderate but significant ellipticities in the range 0.1 < e < 0.25. A significant fraction, 23 per cent, have extreme ellipticities of e > 0.25(and almost all are prolate configurations). About 68 per cent of the proto-haloes are prolate, p > 0, and about 2.3 per cent are extremely prolate, p > 0.25. The average and standard deviation for e and p are 0.206 ± 0.062 and 0.048 ± 0.092 , respectively. It is pretty surprising to note that, despite the pronounced difference of the proto-halo boundaries from iso-density contours about density peaks, the shape distribution of the two are not very different. Bardeen et al. (1986, section VII) quote for overdensity patches about 2.7 σ peaks: 0.17 \pm 0.07 and 0.005 \pm 0.098 for e and p respectively. Using their equations 7.7 and 6.17 for 1σ peaks, which we found to be more appropriate for proto-haloes, we get 0.19 \pm 0.08 and 0.04 \pm 0.11 for e and p respectively.

In §4 we found that the principal axes of the inertia and tidal (and deformation) tensors tend to be aligned, which means that proto-haloes will have their dominant collapse along their major axes of inertia. We now test whether the shape of the proto-halo is correlated with the relative strength of the eigenvalues of the deformation tensor, i.e., the compression factors along the principal axes of \mathcal{D} . In Fig. 7, we show the joint distributions of the ratios i_j/i_k and d_j/d_k between the eigenvalues of the inertia and deformation tensors $(d_i = t_i + \mathcal{D}_{ii}/3)$. Certain correlations are

 $^{^{\}ddagger}$ We deal here with \mathcal{D} rather than T because we expect the self gravity of the proto-halo (described by the diagonal terms of \mathcal{D}) to also play a role in shaping it, as in the basic formulation of the Zel'dovich approximation.

 $[\]S$ We prefer here these ratios over the e and p parameters used to characterize I because the latter are ill-defined for non-positive-

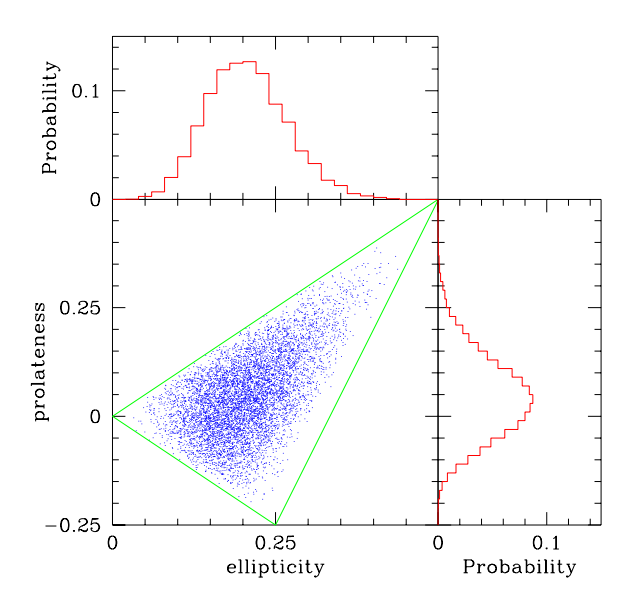


Figure 6. Prolateness and ellipticity for the inertia tensor of proto-haloes. The average and standard deviation values are $\langle e \rangle = 0.206$ and $\sigma_e = 0.062$ and $\langle p \rangle = 0.048$ and $\sigma_p = 0.092$.

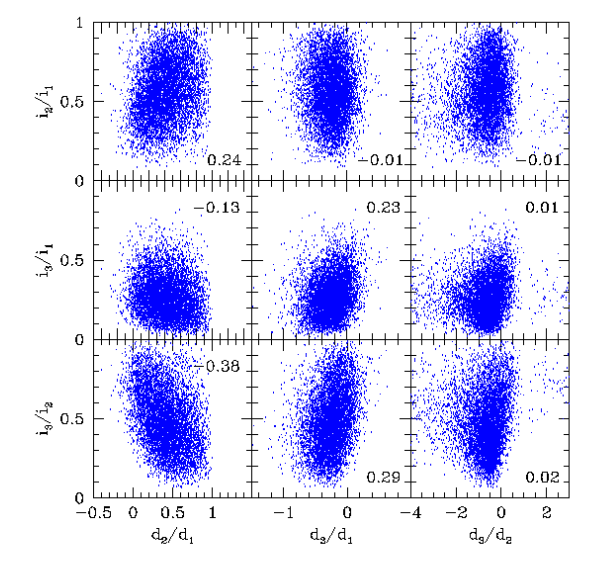


Figure 7. Ratios of the eigenvalues of the inertia tensor versus ratios of the eigenvalues of the deformation tensor (evaluated at the halo centre of mass) for the entire halo population in the simulation. Also shown is the corresponding linear correlation coefficient for the joint distribution in each panel.

detected for some of these ratios, meaning that the degree of asymmetry between the principal axes of the tidal field plays a role in determining the Lagrangian shape of a protohalo. For instance, it appears that the ratio d_2/d_1 is anticorrelated with i_3/i_2 . This may be interpreted as another face of the T-I correlation (§4), where the largest (smallest) compression flow in a proto-halo is associated with its major (minor) axis of inertia. For example, when the two largest compression flows are of comparable strength, $d_1 \sim d_2 > d_3$, the proto-halo configuration is oblate, $i_3 < i_2 \sim i_1$, namely a large d_2/d_1 and a small i_3/i_2 . On the other hand, when the compression is mainly along one axis and $d_2 \simeq 0$ (i.e. small d_2/d_1), the configuration is prolate, $i_3 \sim i_2 < i_1$ (i.e. large i_3/i_2). Note that these correlations, much like the T-I correlation, derive from the constraint that the Lagrangian region is destined to end up in a virialized halo. When pancakes or filaments form instead, the expected correlations may be different, with the final minor axis of inertia correlated with the direction of the largest flow of compression, etc. As seen in Fig. 5, the typical evolution from an initial proto-halo to a final halo indeed passes through an intermediate phase of a pancake (or a filament) lying perpendicular to the direction(s) of first collapse.

Back to proto-haloes, it is clear that binary correlations cannot tell the full story; for a complete study one should consider the joint distribution of the three eigenvalues. Other quantities, such as bulk flows, may also influence the shapes of proto-haloes. Therefore, this issue deserves a more detailed study beyond the scope of the current paper, which only provides first clues.

From the dynamical point of view, proto-haloes can also be classified by the signs of the eigenvalues of the deformation tensor at the centre of mass, indicating whether the initial flows along the principal directions are of compression of dilation. We find that a small minority of the proto-haloes, about 11 per cent, are contracting along all three principal axes. The vast majority, about 86 per cent, are initially collapsing along two directions and expanding along the third. Only 2.7 per cent are collapsing along one direction and expanding along two. This clearly distinguishes the centres of mass of proto-haloes from random points in the Gaussian field, where the probability of the corresponding dynamical configurations based on the deformation tensor would have been 8, 42, and 42 per cent respectively, with the rest 8 per cent expanding along three directions (Doroshkevich 1970). It also distinguishes the proto-haloes from peaks of the lin-

definite matrices such as \mathcal{D} , for which the trace and the single eigenvalues may vanish or be negative.

¶ These fractions are obtained with standard top-hat smoothing of the deformation tensor. Similar numbers (15, 83, 1.5 per cent) are found when only the external velocity field is taken into account and minimal smoothing is applied ($Method\ 3$ of Paper I). However, when the deformation tensor is computed with minimal smoothing and includes the contribution of fluctuations inside the proto-halo ($Method\ 2$), the frequencies become 98.3, 1.7, 0.0 per cent, namely almost all the proto-haloes are collapsing along three spatial dimensions. This is because the local gravitational attraction towards the centre is dominant over the external shear such that it turns the large-scale expansion associated with d_3 (and i_3) into a local contraction. This could be a feature that distinguishes proto-haloes from random patches.

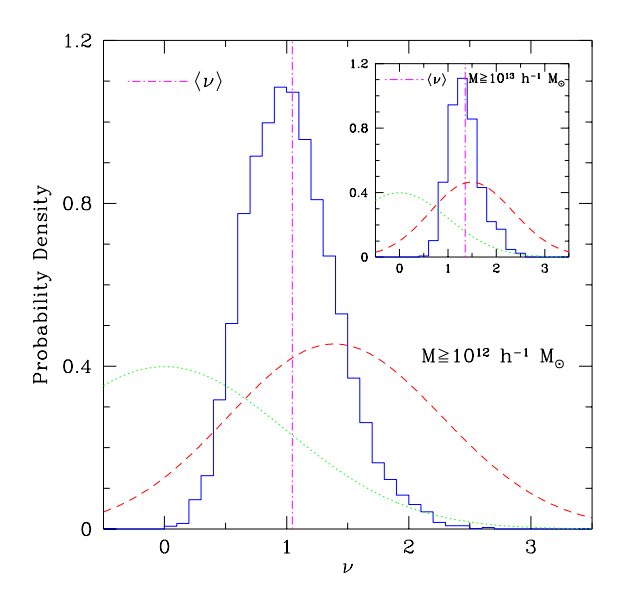


Figure 8. Proto-haloes versus peaks: Distribution of density height $\nu=\delta/\sigma$ at proto-halo centres (solid histogram) versus random points (dotted line) and density maxima (dashed line). The density is smoothed top-hat over the proto-halo scale. The predicted probability distributions for density maxima and for random points are for a corresponding linear Gaussian overdensity field, smoothed on the scale of the smallest halo in the sample. The main panel refers to all the haloes containing more than 100 particles, while the inset refers to haloes of more than 1000 particles. The analytic estimates for peaks practically coincide with the actual density distribution of peaks in our simulation. The averages values, of 1.05 and 1.35, are marked by the dot-dashed lines. The corresponding standard deviations are 0.37 and 0.33, respectively.

ear density field. When smoothed with a top-hat window corresponding to 100 particles, we find in our simulation that the probabilities of the three dynamical configurations are 45, 46 and 8.6 per cent, respectively. These fractions somewhat depend on the smoothing length. Using a top-hat window containing 1000 (10000) particles, the corresponding probabilities become 50 (67), 44 (30) and 5.4 (3.4) per cent. The peaks are characterized by compression along three or two directions, while most of the proto-haloes are compressing along two directions. This finding is consistent with the picture arising from §5 where proto-haloes are typically embedded in elongated, filament-like large-scale structures, surrounded by voids that induce compression flows along the two principal directions orthogonal to the filament.

A certain fraction of our proto-haloes are associated, to some degree, with density peaks in the initial conditions. In Fig. 8 we show the distribution of $\nu=\delta/\sigma$ over all the haloes containing more than 100 (main panel) or 1000 (inset) particles, where δ is the density contrast at the centre of mass of the proto-halo and σ is the rms density contrast over all space. This is compared with the expected distribution of ν , for random points and for density peaks, in a Gaussian random field with the τ CDM power spectrum, smoothed on the scale corresponding to 100 (main panel) and 1000 (inset) particles of our simulation. Note that our proto-haloes typically correspond to one- σ fluctuations with

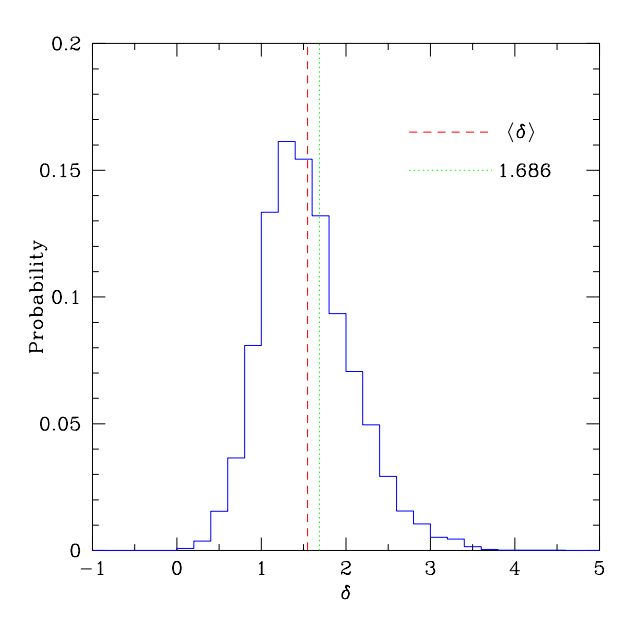


Figure 9. Comparison to the spherical collapse model: Distribution of overdensity for proto-haloes, evaluated at the centre of mass, smoothed top-hat on the halo scale, and linearly extrapolated from the initial conditions to z=0. The average value of the distribution, $\langle \delta \rangle = 1.55$, is marked by the dashed line. The standard deviation of the distribution is 0.54. The value predicted by the spherical collapse model, $\delta \simeq 1.686$, is marked by the dotted line. For haloes with more than 1000 particles, the average is 1.47 and the standard deviation is 0.36.

a relatively small dispersion. This distribution can be clearly distinguished from the density distribution in randomly selected density maxima, which average at about 1.4σ , and have extended tails - especially towards high values. Some of the high peaks are embedded in more extended perturbations of $\nu \sim 1$. They give rise to clumps that eventually merge into the larger haloes that we identify today, and they are therefore not included in our sample of proto-haloes. Also, recall that the impression from Fig. 3 and Fig. 4 was that the correlation between the halo centres of mass and the positions of density peaks is quite limited, and therefore the central proto-halo densities tend to be lower than the heights of the associated peaks. It is also possible that some very high and very low peaks may have deformation configurations that would end up as very aspherical or fragmented structures rather than coherent virialized haloes (e.g. Katz, Quinn & Gelb 1993; van de Weygaert & Babul 1994).

One often uses the terminology of the spherical collapse model to characterize the evolution of proto-haloes. For instance, one refers to 'turnaround' and 'collapse' time, even though, strictly speaking, these quantities are not well-defined for non-spherical objects (see, however, the discussion in Sugerman et al. 2000). One way to test our definition of just-collapsed haloes at z=0, and to address the sphericity of proto-haloes, is by evaluating the accuracy with which the spherical collapse model describes their evolution. Fig. 9 shows the distribution of the linearly extrapolated density contrast at the proto-halo centre of mass, smoothed on the halo size. The average of the distribution, $\delta=1.55$, is within ~ 10 per cent of the standard prediction of the spherical collapse model at collapse time, $\delta \simeq 1.686$. This indicates that

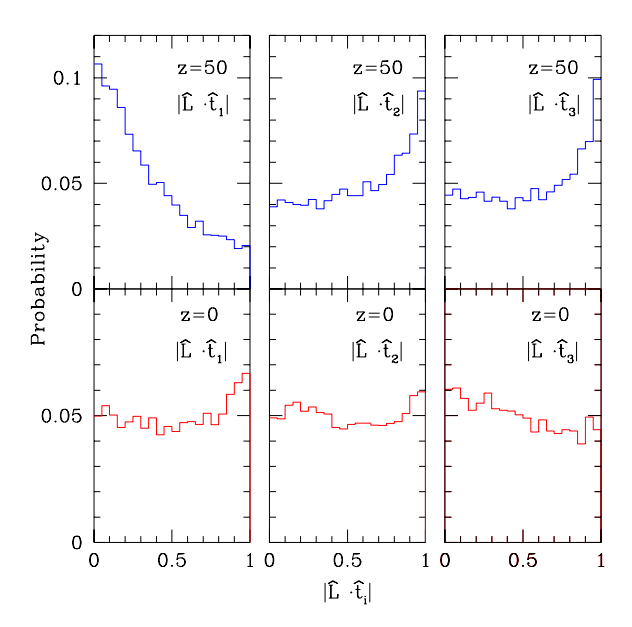


Figure 10. Correlation between halo spin and the linear shear tensor. Shown is the distribution of the cosine of the angle between the halo spin (at z=50 or at z=0) and each of the three eigenvectors of the linear shear tensor. The averages and standard deviations at z=50, for axes 1,2,3 respectively, are: 0.35 ± 0.27 , 0.56 ± 0.30 , 0.55 ± 0.31 . The corresponding values at z=0 are: 0.52 ± 0.30 , 0.50 ± 0.30 , 0.47 ± 0.29 .

our halo finding method and the spherical model are consistent on average. However, the scatter is large, indicating strong deviations from sphericity for many individual protohaloes, which implies a big uncertainty in the turnaround or collapse times.

What are the proto-haloes that populate the tails of the linear overdensity distribution? In particular, how do protohaloes of $\delta \ll 1$ manage to make haloes by today? It is expected that the presence of shear may speed-up the collapse of a density perturbation with respect to the spherical case (Hoffman 1986b; Zaroubi & Hoffman 1993; Bertschinger & Jain 1994). In fact, our haloes with $\delta \ll 1$ are indeed characterized by a strong shear. They typically have $d_1 \simeq -d_3$ and $|d_2| \ll |d_3|$, i.e. they are characterized by compression and dilation factors of similar amplitudes on orthogonal axes. In this case, shear terms in the Raychaudhuri equation (e.g. Bertschinger & Jain 1994) account for significant corrections to the spherical terms, already at z = 50. On the other hand, there are high density proto-haloes, $\delta \sim 3$, which collapse only today, which is late compared to the predictions of the spherical model. These are generally characterized by strong compression flows along 2 directions and by mild expansion along the third axis. The reason for their late collapse is not obvious and deserves further investigation which is beyond our scope here.

7 ALIGNMENT OF SPIN AND SHEAR

Had the inertia and shear tensors been *uncorrelated*, one could have argued that the direction of the spin in the linear regime should tend to be aligned with the direction of

the middle eigenvector of T (and of I). The Cartesian components of L in the frame where T is diagonal are

$$L_i \propto (t_j - t_k) I_{jk} \,, \tag{15}$$

where i, j, k are cyclic permutations of 1, 2, 3. We average over all the possible orthogonal matrices R that may relate the uncorrelated principal frames of T and I, while keeping the eigenvalues of the two tensors fixed, and obtain

$$\langle |L_i| \rangle \propto |t_j - t_k| \langle |I_{jk}| |i_1, i_2, i_3 \rangle = |t_j - t_k| f(i_1, i_2, i_3).$$
(16)

The assumed independence of T and I would have guaranteed that in the principal frame of T the conditional average of I_{jk} (given the eigenvalues of I) would have been the same for all $j \neq k$, namely a certain function $f(i_1,i_2,i_3)$. On average, the largest component $|L_i|$ would have been the one for which $|t_j - t_k|$ is the largest, which is necessarily $L_2 \propto |t_3 - t_1|$, because by definition $t_1 \leq t_2 \leq t_3$. Thus, the angular momentum would have tended to be aligned with \mathbf{t}_2 . To demonstrate this argument and evaluate the strength of the effect, we use the randomized T-I pairs obtained as described at the end of §4. In this case, we find $\langle \hat{\mathbf{L}} \cdot \hat{\mathbf{t}}_i \rangle = 0.40, 0.66, 0.38$ (for i = 1, 2, 3), with a scatter of ~ 0.3 about these mean values. We see that the tendency for alignment with the middle eigenvector is quite significant.

Given that the inertia and shear tensors are in fact strongly correlated (§4), we now investigate, using TTT, what kind of alignment, if any, one should expect between ${f L}$ and T at the initial conditions. Due to the T-I correlation, the distribution of the orthogonal linear transformations R should not be uniform but rather favour rotations with small Euler angles. Moreover, since we saw in §4 that different pairs of eigenvectors have different degrees of alignment, the average off-diagonal terms of I in the principal frame of T would not be all equal anymore. This could be sufficient for drastically changing the preferential alignment of the angular momentum with t_2 seen in the uncorrelated case. Using TTT based on the inertia and tidal tensors for proto-haloes as extracted from the simulation, we actually obtain $\langle \hat{\mathbf{L}} \cdot \hat{\mathbf{t}}_i \rangle = 0.34, 0.59, 0.52$, with a scatter of ~ 0.3 in every case. This shows that the T-I correlation indeed modifies the L-T alignment predicted in the uncorrelated case. The spin tendency for alignment with t_2 is still the strongest, but it is weaker than before. The alignment with \mathbf{t}_3 becomes stronger and almost comparable to the alignment with t_2 , while the alignment with \mathbf{t}_1 becomes even weaker than it was, namely the spin prefers to be perpendicular to \mathbf{t}_1 . We see that, generally speaking, the correlation between I and T tends to weaken the correlation between **L** and T.

Next, we measure the actual spins of the proto-haloes in the initial conditions of the simulation, and correlate it with the directions of the eigenvectors of T. The distributions of angles between these vectors are shown in Fig. 10 (top panels). We see that the spin has a weak but significant tendency to be perpendicular to the major axis of T, and an even weaker tendency to be parallel either to the middle or

Note that a similar argument can be used to show that L would have also been preferentially aligned with the middle eigenvector of I. In this case, however, since all the eigenvalues i_j are positive, one expects a weaker correlation.

to the minor axis of T. In this case, $\langle \hat{\mathbf{L}} \cdot \hat{\mathbf{t}}_i \rangle = 0.35, 0.56, 0.55$, in good agreement with the TTT approximation.

Thus, contrary to LP00, we find no evidence for a strong correlation with the direction of the middle axis of T. LP00 have proposed to parametrize \mathbf{L} -T correlations through the expression

$$\langle \hat{L}_i \hat{L}_j | \hat{T}_{ij} \rangle = \frac{1+a}{3} \delta_{ij} - a \hat{T}_{ik} \hat{T}_{kj} , \qquad (17)$$

where $\hat{T}_{ij} = T_{ij}/[T_{lk}T_{kl}]^{1/2}$ is the trace-free unit shear tensor, and a is the correlation parameter. ** This is particularly convenient for analytical studies of spin statistics (e.g. Crittenden et al. 2001), since it bypasses the ambiguous issue of determining the inertia tensors of proto-haloes and their statistics. The correlation parameter a vanishes if \mathbf{L} is randomly distributed with respect to T, and according to LP00 it should take the value $\sim 3/5$ if TTT holds and T is independent of I (empirically, we actually get $a=0.68\pm0.01$ from the randomized sample in our simulation). It is especially interesting to provide an independent measure of a from our simulation because Eq. (17) has been used in modeling spin-spin correlations (Crittenden et al. 2001) and only one determination of a is available (LP00).

The correlation parameter a can be evaluated in the principal frame of the tidal tensor. Denoting the eigenvalues and eigenvectors of \hat{T} by \tilde{t}_i and $\hat{\mathbf{t}}_i$, one obtains $a=2-6\langle\sum_i(\hat{\mathbf{L}}\cdot\hat{\mathbf{t}}_i)^2\,\tilde{t}_i^2\rangle$, where $\sum\tilde{t}_i^4=1/2$ has been used (LP00). Using this expression for a, we obtain by averaging over all the proto-haloes in our initial conditions $a=0.28\pm0.01$, and when we restrict ourselves to proto-haloes containing 1000 particles or more we get $a=0.33\pm0.04$. It is worth stressing, however, that the dispersion among the proto-haloes of the quantity that is averaged in the determination of a is very large, with an rms value of about 0.9, which is not a good property of this statistic.

Next, we wish to find out how much of the (weak) L-T correlation detected at the initial conditions actually survives the non-linear evolution to the present epoch. For this we plot in the bottom panels of Fig. 10 the distributions of angles between the final spin and the initial shear tensor. We find that the correlation is strongly weakened. This is hardly surprising based on the significant non-linear evolution in spin direction found in Paper I. We obtain $a = 0.07 \pm 0.01$, at variance with the result obtained by LP00, $a = 0.24 \pm 0.02$ at z = 0, using a low-resolution particle-mesh simulation of an $\Omega = 1$ CDM model. Our result persists when considering only the haloes containing 1000 particles or more, $a = 0.07 \pm 0.04$. The discrepancy with LP00 is probably an effect of the higher accuracy with which our high-resolution, adaptive P³M code accounts for non-linear effects. The smoothing length used to define \hat{T}_{ij} in the simulation could also affect the results (for instance, smoothing on too small a scale might give unphysically small L-T correlations). In order to test the dependence of our findings on the adopted filtering radius, we re-compute a using a top-hat window function which contains 8 times the halo mass. In this case, for haloes with 100 particles or more, we find $a=0.24\pm0.01$ at z=50, and $a=0.08\pm0.01$ at z=0. This shows that smoothing is not a major issue here.

Our result above seems to suggest that observed spin directions, as deduced from disc orientations, cannot be used to deduce useful information about the initial shear tensor. How relevant are our results to the orientation of disc galaxies? On one hand, the haloes in our current analysis are all characterized by a present-day overdensity of \sim 180, while the galactic discs are associated with much higher density contrasts, so a certain unknown extrapolation is required. Moreover, it is plausible that the plane of today's disc galaxy is determined by the halo spin at an early time, before the gas fell into the disc. As expected, we see in the simulation that the non-linear effects wipe out the spin-shear correlation in a gradual fashion, e.g., $a = 0.26, 0.20, 0.11 \ (\pm 0.01)$ at z = 1.2, 0.6, 0.2 respectively. Therefore, the disc orientation may after all preserve some of the weak correlation with the initial shear field, and this should be true especially for galaxies that formed at high redshift. On the other hand, we know that the spin and shear are correlated better at high redshift only for the haloes that we selected at z = 0, and we do not know whether this is true for the subhaloes which host disc formation at higher redshift. It is also possible that the statistical orthogonality between the spin and the first principal shear axis is preserved better in specific regions were cosmic flows are particularly cold. The cold-flow neighborhood of the Local Group might provide a suitable field for studying such a correlation. Still, we expect only a weak correlation.

8 CONCLUSION

In order to deepen our understanding of how tidal torques actually work, we investigated the cross-talk between the main components of the theory using ~ 7300 well-resolved haloes extracted from a cosmological N-body simulation. We studied the correlation between the proto-halo inertia tensor and the external shear tensor, and between them and the spin direction, and tried to characterize the proto-halo regions in several different ways. We defined haloes in today's density field using the standard friends-of-friends algorithm, but it would be useful for future work to check robustness to alternative halo finders as well as to different cosmological scenarios.

We found to our surprise that the T and I tensors are strongly correlated, in the sense that their minor, major and middle principal axes tend to be aligned, in this order. This means that the angular momentum, which plays such a crucial role in the formation of disc galaxies, is only a residual which arises from the little, $\sim \! 10$ per cent deviations from perfect alignment of T and I.

The T-I correlation induces a weak tendency of the proto-halo spin to be perpendicular to the major axis of T (and I). It also slightly weakens the spin tendency to be aligned with the middle axis (a tendency that would have dominated had T and I been uncorrelated) and slightly strengthen its alignment with the minor axis. However, these correlations, even at the initial conditions, are weak. Fur-

^{**} We notice that the claim of LP00, that Eq. (17) represents the most general quadratic relation between a unit vector and a unit tensor, is not formally true, because, for example, Eq. (17) cannot describe the case where $\hat{\mathbf{L}}$ systematically lies along one of the principal axes of T. However, since this configuration cannot be realized in TTT, we adopt Eq. (17) as a plausible parametrization of the correlation.

thermore, non-linear changes in spin direction at late times practically erase the memory of the initial shear tensor, and therefore observed spin directions cannot serve as very useful indicators for the initial shear tensor (again, in variance with LP00). The only partial caveat is that today's discs may reflect the halo spin directions at some high redshift, which may still preserve some weak correlation with the linear shear field. A study of this effect would require a high-resolution simulation in which a detailed galaxy formation scheme is incorporated.

On the other hand, the strong $T\!-\!I$ correlation provides a promising hint for how to make progress in a long-standing open question in galaxy formation theory. That is, how to characterize proto-haloes and their boundaries. Speculations based on iso-density or iso-potential contours about highdensity peaks have failed the tests of simulations. We first realize that the centres of proto-haloes tend to lie in $\sim 1\sigma$ over-density regions, but their association with the linear density maxima smoothed on galactic scales is quite limited. We find that the proto-haloes tend to be elongated along the direction of maximum compression of the smoothed velocity field. A typical configuration is of an elongated proto-halo lying perpendicular to an elongated background density ridge, with neighboring voids inducing the compression along the major and intermediate inertia axes. The T-I correlation detected here should thus enable the construction of a detailed algorithm to identify proto-haloes and their boundaries in cosmological initial conditions (Porciani, Dekel & Hoffman, in preparation).

The collapse proceeds in two succesive stages, corresponding to the quasi-linear and the non-linear regimes. The first stage is characterized by a two dimensional collapse in the plane defined by the major and intermediate inertia axes. This leads to the formation of a transient clumpy elongated structure aligned with the large scale filament within which the halo resides. In the fully non-linear regime the protohalo experiences a one-dimensional collapse and a series of merger of the sub-clumps along the filament, leading to a quasi-spherical object in virial equilibrium.

The proto-haloes can be characterized by a variety of other statistics, which may distinguish them from overdensity patches about random density peaks. In terms of shape, most proto-haloes have significant ellipticities and most of them are prolate, but this does not distinguish them very clearly from over-density patches about peaks. In contrast with the strong alignment of the inertia and deformation tensors, there are only weak correlations between the triaxiality of the inertia tensor and that of the deformation tensor, as expressed by ratios of eigenvalues.

The vast majority of proto-haloes are initially collapsing along two principal directions (except when the self gravity is also considered, inducing a collapse in all directions). This is in clear contrast with the behaviour of density peaks, which have similar probabilities to collapse along three or two axes. Our finding is consistent with proto-haloes being embedded in large-scale filaments surrounded by voids. The smoothed central densities in proto-haloes typically represent 1σ positive perturbations, but with smaller dispersion than for general peaks. This is partly because the proto-halo centers are only weakly correlated with the density peaks, and also because some of the high peaks lead to clumps that later merge into the big haloes we identify today and include

in our sample. Despite the significant asphericity, the protohalo densities agree on average with the predictions of the spherical collapse model, but the scatter is large. For example, there are proto-haloes with $\delta \ll 1$ (with δ the density contrast smoothed on the halo scale and linearly estrapolated to today), whose collapse is boosted by strong shear of large compression and dilation factors.

In Paper I, we evaluated the performance of linear TTT in predicting the spin of galactic haloes. We found that, for a given proto-halo at the initial conditions, TTT provides a successful order-of-magnitude estimate of the final halo spin amplitude. The TTT prediction matches on average the spin amplitude of today's virialized haloes if linear TTT growth is assumed until about $t_0/3$. This makes TTT useful for studying certain aspects of galaxy formation, such as the origin of a universal spin profile in haloes (Bullock et al. 2001b; Dekel et al. 2001), but only at the level of average properties, because the random error is comparable with the signal itself. We also found in Paper I that non-linear evolution causes significant variations in spin direction, which limit the accuracy of the TTT predictions to a mean error of $\sim 50^{\circ}$. Furthermore, spatial spin-spin correlations on scales $\geq 1 h^{-1}$ Mpc are strongly weakened by non-linear effects. This limits the usefulness of TTT in predicting intrinsic galaxy alignments in the context of weak gravitational lensing (Catelan et al. 2001; Crittenden et al. 2001). This situation may improve (as in the case of the spin-shear correlation addressed in the current paper) if the orientations of today's discs were determined by the halo spins at a very high redshift, which are better modelled by TTT. On the other hand, we know this only for the haloes that we selected at z=0, and we don't know whether this is true for the subhaloes which host disc formation at higher redshift.

In our studies of the cross-talk between the different components of TTT, we have also realized another surprise that leads to a revision in the standard scaling relation of TTT (White 1984). It is demonstrated in Paper III that the off-diagonal, tidal terms of the deformation tensor, which drive the torque, are only weakly correlated with the diagonal terms, which determine the overdensity at the protohalo centre. The latter enters the TTT scaling relation via the expected collapse time of the proto-halo, and the lack of correlation with the torque leads to a modification in the scaling relation. The revised scaling relation can be applied shell by shell in order to explain the origin of the universal angular-momentum profile of haloes (Bullock et al. 2001b; Dekel et al. 2001). It can also be very useful in incorporating spin in semi-analytic models of galaxy formation (Maller, Dekel & Somerville 2002).

ACKNOWLEDGMENTS

This research has been partly supported by the Israel Science Foundation grants 546/98 and 103/98, and by the US-Israel Binational Science Foundation grant 98-00217. CP acknowledges the support of a Golda Meir fellowship at HU and of the EC RTN network 'The Physics of the Intergalactic Medium' at the IoA. We thank our GIF collaborators, especially H. Mathis, A. Jenkins, and S.D.M. White, for help with the GIF simulations.

REFERENCES

Bardeen J.M., Bond J.R., Kaiser N., Szalay, A. S., 1986, ApJ, 304, 15

Barnes J., Efstathiou G., 1987, ApJ, 319, 575

Bertschinger E., Jain B., 1994, ApJ, 431, 486

Bond J.R., Efstathiou G., 1991, Phys. Lett. B, 265, 245

Bond J.R., Myers S.T., 1996, ApJS, 103, 1

Bullock J.S., Kolatt T.S., Sigad Y., Somerville R.S., Kravtsov A.V., Klypin A.A., Primack J.R., Dekel A., 2001a, MNRAS, 321, 559

Bullock J.S., Dekel A., Kolatt T.S., Kravtsov A.V., Klypin A.A., Porciani C., Primack J.R., 2001b, ApJ, 555, 240

Catelan P., Theuns T., 1996, MNRAS, 282, 436

Catelan P., Porciani C., 2001, MNRAS, 323, 713

Catelan P., Kamionkowski M., Blandford R., 2001, 320, L7

Colberg, J.M., White, S.D.M., Jenkins, A. & Pearce, F.R. 1999, MNRAS, 308, 593

Crittenden R.G., Natarajan P., Pen U., Theuns T., 2001, ApJ, 559, 552

Croft, R.A.C., Metzler C.A., 2000, ApJ, 545, 561

Dekel A., Bullock J.S., Porciani C., Kravtsov A.V., Kolatt T.S., Klypin A.A., Primack J.R., 2000, in J.G. Funes S.J., E.M. Corsini, eds. Galaxy Disks and Disk Galaxies, ASP Conference Series, astro-ph/0011002

Doroshkevich A.G., 1970, Astrofizika, 6, 581

Efstathiou G., Eastwood J.W., 1981, MNRAS, 194, 503

Heavens A., Peacock J.A., 1988, MNRAS, 232, 339

Heavens A., Refregier A., Heymans C., 2000, 319, 649

Hoffman Y., 1986a, ApJ, 301, 65

Hoffman Y., 1986b, ApJ, 308, 493

Hoffman Y., 1988a, ApJ, 329, 8

Hoffman Y., 1988b, ApJ, 328, 489

Hoyle F., 1949, Burgers J.M., van de Hulst H.C., eds., in Problems of Cosmical Aerodynamics, Central Air Documents Office, Dayton, p. 195

Katz N., Quinn T. & Gelb J., 1993, MNRAS, 265, 689

Kauffmann G., Colberg J.M., Diaferio A., White S.D.M., 1999, MNRAS, 303, 188

Lee J., Pen U., 2000, ApJ, 532, L5 (LP00)

Lin C.C., Mestel L., & Shu F.H., 1965, ApJ, 142, 1341

Maller, A., Dekel, A., & Somerville, R., 2002, MNRAS, 329, 423

Navarro J.F., Frenk C., & White S.D.M., 1995, MNRAS, 275, 56

Navarro J.F., & Steinmetz M., 1997, ApJ, 478, 13

Navarro J.F., & Steinmetz M., 2000, ApJ, 538, 477

Pearce F.R., Couchman H.P.M., 1997, astro-ph/9703183

Pearce F.R., Couchman H.P.M., Jenkins A.R., Thomas P.A., 1995, Hydra–Resolving a Parallel Nightmare, in Dynamic Load Balancing on MPP systems

Peebles P.J.E., 1969, ApJ, 155, 393

Pen U., Lee J., & Seljak U., 2000, ApJ, 543, 107

Porciani, C., Dekel, A., Hoffman, Y., 2001, MNRAS, submitted, astro-ph/0105123 (Paper I)

Sigad, Y., Kolatt, T.S., Bullock, J.S., Kravtsov, A.V., Klypin, A.A., Primack, J.R., & Dekel A., 2001, MNRAS, submitted

Steinmetz M., Bartelmann M., 1995, MNRAS, 272, 570

Sugerman B., Summers F.J., Kamionkowski M., 2000, MNRAS, 311, 762

van de Weygaert R., & Babul A., 1994, ApJ, 425, L59

White S.D.M., 1984, MNRAS, 286, 38

White S.D.M., 1996, Schaeffer R., Silk J., Spiro M., Zinn-Justin J., eds., in Cosmology and Large-scale Structure, Elsevier, Dordrecht, The Netherlands, p. 349
Bernstein G., 2000, Nature, 405, 143

Zaroubi, S. & Hoffman, Y., 1993, ApJ, 414, 20

Zel'dovich Ya.B., 1965, MNRAS, 129, 19

Zel'dovich Ya.B., 1970, Astr. Ap., 5, 84

This paper has been produced using the Royal Astronomical Society/Blackwell Science IATEX style file.